Photonic crystal fiber mapping using Brillouin echoes distributed sensing

B. Stiller,[1] S. M. Foaleng,[2] J.-C. Beugnot,[2] M. W. Lee,[1] M. Delqué,[1] G. Bouwmans,[3] A. Kudlinski,[3] L. Thévenaz,[2] H. Maillotte,[1] and T. Sylvestre[1]

[1]*Institut FEMTO-ST, Université de Franche-Comté, F-25030 Besançon, France*
[2]*Group for Fibre Optics, École Polytechnique Fédérale de Lausanne, CH-1015 Switzerland*
[3]*Université Lille 1, IRCICA, Laboratoire PhLAM, 59655 Villeneuve d'Ascq, France*
**birgit.stiller@femto-st.fr*

Abstract: In this paper we investigate the effect of microstructure irregularities and applied strain on backward Brillouin scattering by comparing two photonic crystal fibers drawn with different parameters in order to minimize diameter and microstructure fluctuations. We fully characterize their Brillouin properties including the gain spectrum and the critical power. Using Brillouin echoes distributed sensing with a high spatial resolution of 30 cm we are able to map the Brillouin frequency shift along the fiber and get an accurate estimation of the microstructure longitudinal fluctuations. Our results reveal a clear-cut difference of longitudinal homogeneity between the two fibers.

OCIS codes: (060.2270) Fiber characterization; (060.2280) Fiber design and fabrication; (060.2370) Fiber optics sensors; (060.4005) Microstructured fibers; (060.5295) Photonic crystal fibers; (290.5830) Scattering, Brillouin.

References and links

1. E. P. Ippen, and R. H. Stolen, "Stimulated Brillouin scattering in optical fibers," Appl. Phys. Lett. **21**(11), 539–541 (1972).
2. M. Niklès, L. Thévenaz, and P. A. Robert, "Simple distributed fiber sensor based on Brillouin gain spectrum analysis," Opt. Lett. **21**(10), 758–760 (1996).
3. L. Thévenaz, "Brillouin distributed time-domain sensing in optical fibers: state of the art and perspectives," Front. Optoelectron. China **3**(1), 13–21 (2010).
4. L. Zou, X. Bao, and L. Chen, "Distributed Brillouin temperature sensing in photonic crystal fiber," Smart Mater. Struct. **14**(3), S8 (2005).
5. P. Dainese, P. S. J. Russell, N. Joly, J. C. Knight, G. S. Wiederhecker, H. L. Fragnito, V. Laude, and A. Khelif, "Stimulated Brillouin scattering from multi-GHz-guided acoustic phonons in nanostructured photonic crystal fibres," Nat. Phys. **2**(6), 388–392 (2006).
6. A. Minardo, R. Bernini, W. Urbanczyk, J. Wojcik, N. Gorbatov, M. Tur, and L. Zeni, "Stimulated Brillouin scattering in highly birefringent microstructure fiber: experimental analysis," Opt. Lett. **33**, 2329–2331 (2008).
7. J.-C. Beugnot, T. Sylvestre, D. Alasia, H. Maillotte, V. Laude, A. Monteville, L. Provino, N. Traynor, S. Foaleng Mafang, and L. Thévenaz, "Complete experimental characterization of stimulated Brillouin scattering in photonic crystal fiber," Opt. Express **15**(23), 15517–15522 (2007), `http://www.opticsinfobase.org/abstract.cfm?uri=oe-15-23-15517`.
8. M. Karlsson, "Four-wave mixing in fibers with randomly varying zero-dispersion wavelength," J. Opt. Soc. Am. B **15**(8), 2269–2275 (1998).
9. M. Niklès, L. Thévenaz, and P. A. Robert, "Brillouin gain spectrum characterization in single-mode optical fiber," J. Lightwave Technol. **15**(10), 1842–1851 (1997).
10. R. G. Smith, "Optical power handling capacity of low loss optical fibers as determined by stimulated Raman and Brillouin scattering," Appl. Opt. **11**(11), 2489 (1972).

#130909 - $15.00 USD Received 29 Jun 2010; revised 31 Aug 2010; accepted 31 Aug 2010; published 7 Sep 2010

11. G. P. Agrawal, *Nonlinear fiber optics*, 3rd ed. (Academic Press, 2001).
12. M. O. V. Deventer and A. J. Boot, "Polarisation properties of stimulated Brillouin scattering in single mode fibers," J. Lightwave Technol. **12**(4), 585–590 (1994).
13. R. Boyd, K. Rzazewski and P. Narum, "Noise initiation of stimulated Brillouin scattering," Phys. Rev. A **42**(9), 5514–5521 (1990).
14. S. L. Floch and P.Cambon, "Theoretical evaluation of the Brillouin threshold and the steady-state Brillouin equations in standard single-mode optical fibers," J. Opt. Soc. Am. A **20**(6), 1132–1137 (2003).
15. S. Foaleng Mafang, J.-C. Beugnot and L. Thévenaz, "Optimized configurarion for high resolution distributed sensing using Brillouin echoes," Proc. SPIE, UK, Edinburgh *75032C*, 7503 (2009).
16. F. Poletti, K. Furusawa, Z. Yusoff, N. G. R. Broderick, and D. J. Richardson, "Nonlinear tapered holey fibers with high stimulated Brillouin scattering threshold and controlled dispersion," J. Opt. Soc. Am. B **24**(9), 2185–2194 (2007).
17. Crystal Fibres, `http://www.nktphotonics.com/`.
18. T. G. Euser, J. S. Y. Chen, M. Scharrer, P. S. J. Russell, N. J. Farrer, and P. J. Sadler, "Quantitative broadband chemical sensing in air-suspended solid-core fibers," J. Appl. Phys. **103**, 103108 (2008).

1. Introduction

Brillouin Scattering in optical fibers results from the interaction between light and acoustic waves through the effects of electrostriction [1]. The Brillouin gain and Brillouin frequency shift (BFS) depend on the overlap of these waves in the fiber core and on the material. Temperature and strain influence the velocity of the acoustic wave and thus the BFS. Since the acoustic modes are sensitive to temperature and strain, Brillouin backscattering has widely been studied for distributed sensing in single mode fibers (SMF) [2, 3] as well as in photonic crystal fibers (PCF) [4]. Due to their high nonlinear efficiency, PCFs have received particular attention for temperature and strain sensing. It has recently been reported that PCF with small core exhibit in most cases a multi-peak Brillouin spectrum due to the periodic air-hole microstructure [5–7]. This aspect could be advantageously used for simultaneous strain and temperature distributed measurements. However, when multi peaks overlap, the spectrum broadens and the data analysis becomes more difficult. Another aspect that limits distributed measurements is the inhomogeneity of opto-geometrical parameters along the fiber which has an influence on the BFS. This is even more crucial in PCFs since their fabrication requires an accurate control of more parameters than for SMF during the drawing process. In this work we fully characterize two PCFs with the nearly same air-hole microstructure but drawn with different parameters in order to minimize diameter fluctuations. The experiments presented in this work are twofold: we first perform an integrated measurement of the Brillouin gain spectrum (BGS) and the critical power (also called Brillouin threshold) and then a Brillouin-echoes distributed sensing (BEDS) measurement. Our results show that these two fibers exhibit a single peak in the gain spectrum like an SMF and that their critical powers of stimulated scattering are in good agreement with theory. The impact of structural irregularities and strain on the BFS is also clearly evidenced. We observe in particular long- and short-scale fluctuations in the BFS. Although short-scale longitudinal fluctuations were studied in Ref. [8], it is the first time that the short-scale fluctuations are investigated in optical fibers using the BEDS technique. We further show that it is possible to extract the effective refractive index all along the fiber from the distributed BFS measurements, which allows a quantitative estimation of fiber irregularities. With these measurements we are able to draw conclusions about the fiber inhomogeneity induced by the drawing process.

2. Experimental results

The two PCFs under test have a hexagonal hole structure and their cross-sections are shown in the insets of Fig. 1. They originate from the same stack, but from different intermediate canes. The cane used to manufacture fiber #1 was 3.8 mm in outer diameter and drawn at a relatively

#130909 - $15.00 USD Received 29 Jun 2010; revised 31 Aug 2010; accepted 31 Aug 2010; published 7 Sep 2010

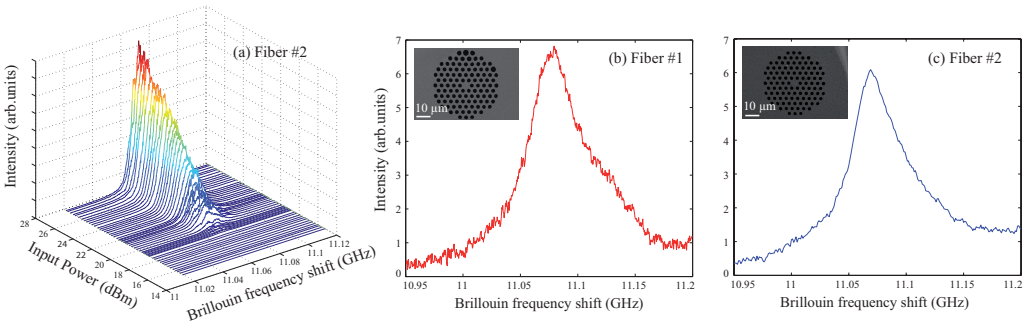

Fig. 1. (a) Brillouin gain spectrum for fiber #2 with increasing input power. Brillouin spectrum for an input pump power of 11 dBm, which is under the critical power, for (b) fiber #1 and (c) fiber #2. The PCF cross-sections are shown in the insets.

high temperature (low tension). For fiber #2 the cane was drawn with the same parameters, except for the temperature that was much lower than for fiber #1, leading to a much higher tension during the drawing process. At this stage, the outer diameter fluctuations of both canes were comparable, but the air holes were slightly smaller in cane #1 than in cane #2. The canes were then inserted into jacketing tubes, and drawn down into fibers. Both fibers were drawn with comparable parameters, although a slightly higher pressure was used for fiber #1 to inflate air holes. The outer diameter fluctuations measured during the drawing process were about 2% for fiber #1 and less than 1% for fiber #2. Both of the fibers are designed to get a zero-dispersion-wavelength around 1060 nm and have an attenuation of 5 dB/km (#1) and 8.6 dB/km (#2) at 1.5 µm. Their effective mode area (EMA) is about 15 μm^2 (#1) and 16 μm^2 (#2) at 1.5 µm found by calculation based on scanning electron microscopy (SEM) images. The core, hole diameter, pitch, and length are about 5.5 µm, 2.7 µm, 4.1 µm, 100 m for fiber #1 and 5.5 µm, 2.3 µm 3.9 µm, 400 m for fiber #2.

2.1. Brillouin gain spectrum

Before the distributed analysis of the BFS along the fibers we have first performed a direct measurement of the gain spectrum and the critical power using the same experimental setup as in Ref. [7]. Since in the latter case the scattered light is affected by strain, differences of temperature and air-hole microstructure fluctuations along the fiber, it is called integrated measurement. As an example, the Brillouin spectrum dynamics in function of the pump power obtained from fiber #2 is shown in Fig. 1(a). The full width at half maximum (FWHM) for fiber #1 and #2 narrows from 55 MHz and 60 MHz respectively in the spontaneous regime to 10 MHz in the stimulated one. For comparison the FWHM in a single-mode fibers (SMF) in the spontaneous regime is about 27 MHz [9]. This Brillouin linewidth broadening is due to fiber inhomogeneities and to the photonic crystal cladding that allows the simultaneous generation of several longitudinal acoustic modes, as previously demonstrated [7]. To get better insight, Fig. 1(b) and 1(c) show the Brillouin spectra at 11 dBm which is below the critical power of stimulated scattering. One can see that there exists a single peak as in an SMF and an asymmetry in the spectra can be noticed, particularly for fiber #1. This asymmetry suggests the presence of two or more acoustic modes with close Brillouin frequency shift and thus overlaping gain spectra. Let us now briefly recall the relation that links the BFS to the effective refractive index of the fiber that reads [9]:

$$\nu_B = \frac{2n_{\text{eff}}V_L}{\lambda_P} \tag{1}$$

For a refractive index of $n_{\text{eff}} \approx n = 1.44$ and an acoustic velocity of $V_L = 5960$ m/s (longitu-

#130909 - $15.00 USD Received 29 Jun 2010; revised 31 Aug 2010; accepted 31 Aug 2010; published 7 Sep 2010

dinal) the frequency of the Stokes wave is shifted by $\nu_B = 11.07$ GHz at $\lambda_P = 1.55$ μm pump wavelength, in very good agreement with the measured Brillouin spectra shown in Fig. 1.

2.2. *Critical power of stimulated Brillouin scattering*

The critical power is also measured for the two fibers. The estimated value for the critical power is given by [10]:

$$P_{\mathrm{cr}} = \frac{C \cdot K \cdot A_{\mathrm{eff}}}{g_B \cdot L_{\mathrm{eff}}} \tag{2}$$

where A_{eff} is the EMA, L_{eff} the effective length, C=21 and g_B the Brillouin gain. The Brillouin gain can be determined by measuring the FWHM in the spontaneous Brillouin regime [1]. For fiber #1 the Brillouin gain is $g_B = 1.25 \cdot 10^{-11}\ mW^{-1}$ and for fiber #2 we obtain $g_B = 1.15 \cdot 10^{-11}\ mW^{-1}$. The value of K depends on the fiber type. In a polarization maintaining fiber K=1 whereas in an SMF K=3/2 as the polarization changes randomly [12]. This definition assumes that the critical power is reached when the reflected Stokes power equals the transmitted power. However, for practical reasons the critical power can be defined at the point where the reflected power is 1% of the injected one [13]. This requires to modify Eq. (2). The numerical factor 21 is approximately the natural logarithm of the gain [10]. Floch et al. [14] adjusted this factor depending on the fiber length. Adapting the equation to the 1%-definition changes the numerical factor C depending on fiber length and attenuation to 15.5 for fiber #1 and 16 for fiber #2 which is obtained by numerical approximations. With the measured and calculated values the theoretical critical power can be estimated at 25.1 dBm for fiber #1 and 20.2 dBm for fiber #2. The critical power for stimulated scattering is measured with the same setup as for the Brillouin spectrum without the heterodyne detection [7]. The results for the backscattered and transmitted power depending on the input power for both fibers are shown in Fig. 2. The experimental value of the critical power is obtained as 26.7 dBm for fiber #1 and 20.2 dBm for fiber #2 taking into account splicing losses of about 1.5 dB. Comparing the theoretical values with the experimental ones we found them in good agreement for both fibers. Assuming the fairly high birefringence in those fibers, the factor 3/2 is probably too large, Fiber #1 being shorter. This may be a tentative explanation of the discrepancy with Fiber #1.

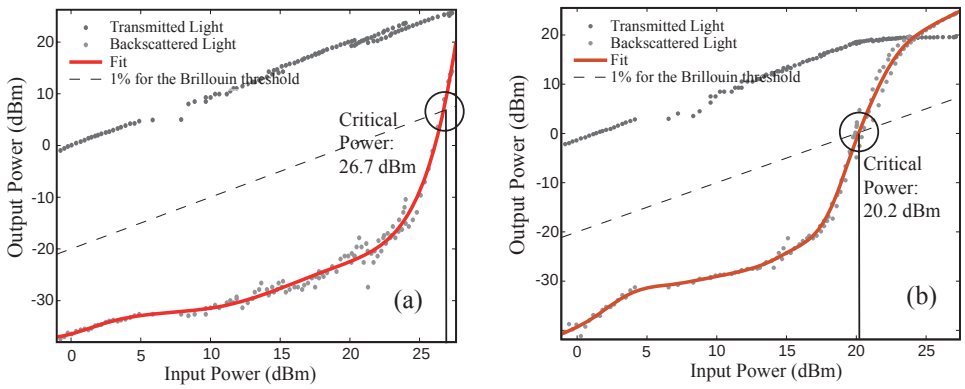

Fig. 2. Backscattered and transmitted power versus input power of (a) fiber #1 and (b) fiber #2

[1] using $g_B = \frac{2\pi n^7 p_{12}^2}{c\lambda_P^2 \rho_0 v_A \Delta\nu_B}$ [11]

#130909 - $15.00 USD Received 29 Jun 2010; revised 31 Aug 2010; accepted 31 Aug 2010; published 7 Sep 2010

2.3. *Distributed Sensing using Brillouin Echoes*

The BEDS technique basically differs from a conventional Brillouin optical time domain analysis (BOTDA) [2]. Indeed, the distributed measurement of precise Brillouin gain spectrum (BGS) can be made with enhanced spatial resolution by applying short π-phase shifts in the CW pump wave instead of using rectangular intensity pulses. This configuration offers the advantage to measure a gain spectrum unaltered by the pump spectrum and to experimentally estimate the acoustic lifetime. The experimental setup is schematically shown in Fig. 3(a) and a complete description of the method can be found in Refs. [3, 15]. The output of an external cavity laser at 1551 nm is split into two arms by a polarization-maintaining coupler. One arm serves for the cw probe and the other one for the pump. An intensity modulator, driven by a microwave generator, creates two sidebands tuned to the BFS of the two PCF measured above.

The probe wave is then amplified by an EDFA and injected into the PCF. The other arm is connected to the opposite end of the PCF through an optical circulator. The pump wave is modulated at a 10 kHz repetition rate via a phase modulator driven by a pulse generator. A π-phase shift is applied on the pump for a 3-ns short time, so that the reflected Stokes light interferes destructively with the probe signal, equivalent to a Brillouin loss process. A tunable fiber Bragg grating (FBG) connected to a second optical circulator filters out the Stokes-wave and residual pump light. The output cw probe is then monitored with an oscilloscope while it is scanned around the BFS so that all BFS shifts due to inhomogeneities and strain can be detected. The spatial resolution is about 30 cm which is determined by the pulse duration. Since the acoustic wave has a finite lifetime of several ns the backscattered response of the BEDS system is partially decaying during the phase pulse duration. This creates a second echo when the pump is restored to its original state after the pulse [15]. To avoid this undesirable effect we turn off the pump immediately after the phase pulse so that no more light can be reflected after the pulse end and no trailing light is present [3]. This is achieved by adding in the experimental setup a second intensity modulator before the phase modulator to produce a pump intensity pulse of 30 ns with a π phase pulse (3 ns) at its end. Fig. 3(b) illustrates the result of the BEDS measurement for fiber #1 while the probe modulation frequency is swept around the BFS. The data were averaged and fitted by using a convolution with a rectangle to reduce measurement noise. Figure 3 gets further insight into the longitudinal fluctuations of the BFS. As it can be seen, the distributed BFS exhibit both long- and short scale longitudinal fluctuations that are due to diameter fluctuations. Particularly for fiber #1 we can identify a long-scale sinusoidal variations of about 8 MHz with a half-period of approximatively 50 m that corresponds to the middle of the fiber. This BFS variation is due to the strain induced by the fiber coiling as a half of the fiber length is coiled on the other half. This was easily confirmed

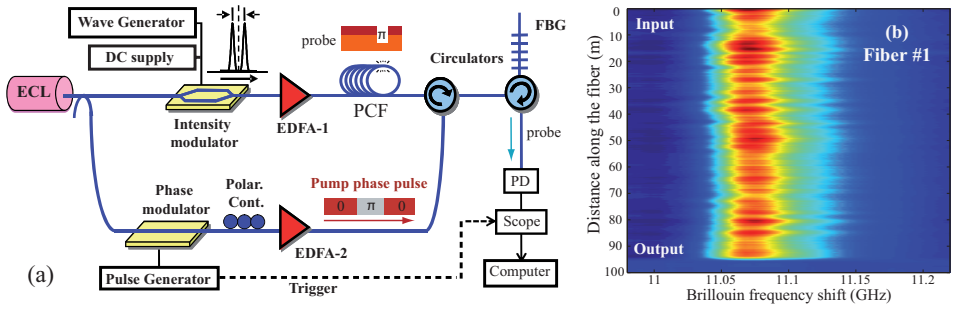

Fig. 3. (a) Experimental setup of the BEDS system. ECL: external cavity laser; EDFA: erbium-doped fiber amplifier; PD: photodiode. (b) Color plot of Brillouin frequency shift along fiber #1. The spatial resolution is 30 cm and the frequency resolution is 2 MHz.

#130909 - $15.00 USD Received 29 Jun 2010; revised 31 Aug 2010; accepted 31 Aug 2010; published 7 Sep 2010

by inverting the PCF in the setup. On the other hand, the short-scale longitudinal fluctuation (about 5±1 MHz every 2 m) seen in Fig. 4(a) indicates a random geometric variation of the air-hole microstructure. Note that this cannot be attributed to the influence of birefringence in the PCF since the variation on the refractive index can be estimated to $7 \cdot 10^{-4}$ using Eq. (1) which is well above the birefringence of the PCF (estimated phase birefringence by simulation: $\approx 1.5 \cdot 10^{-5}$, measured group birefringence: $\approx 5 \cdot 10^{-6}$). Figure 4(b) shows a 5 MHz shift in BFS for fiber #2 between 80 m and 180 m which corresponds to one layer of the fiber coil. In this way we are able to detect the strain applied to one layer. The short scale fluctuation is smaller (3±1 MHz, every 2-3 m of the fiber) and can be attributed to geometrical fluctuations of the air-hole microstructure.

It is clear from Fig. 4 that the longitudinal fluctuations in BFS are less significant for fiber #2 than fiber #1 as the drawing process was better controlled. This is verified by studying the fast Fourier transform of the BFS trace shown in the insets of Fig. 4. We notice that for fiber #1 the frequencies pedestal around the main peak is wider than for fiber #2. In order to obtain an estimation of the diameter or microstructure fluctuations along the fibers, we have derived the distributed effective refractive index n_{eff} from the distributed BFS as they are proportionately linked by Eq. (1) (V_L and λ_P are known). In the following, we assume that the main contributions to these fluctuations are due to homothetic variations of the microstructure, i.e. to fluctuations of the outer diameter only. We neglect here possible longitudinal inhomogeneities of individual air holes or pitch, as well as possible twists induced during the drawing process because of several reasons. The variation of the effective refractive index can derive from different origins: applied strain, temperature variation, longitudinal variations of the microstructure, individual air holes inhomogeneities or variation of the pitch. We assume that the temperature do not influence the experiment because of the short experiment duration. The impact of strain is observed in long scale fluctuations which indicate the effect of the fiber coiling. Moreover the variation of the pitch has an important impact on the effective refractive index, which can be found in Ref. [16]. However several SEM-images at different sections of the fibers show that there is no measurable variation of the pitch and singular air holes. From our numerical simulation using Comsol it is found that the variation of the microstructure scale is the main cause of the variation of the effective refractive index. So we decided to vary the scale of the microstructure since this seemed to be the most general variation. To relate geometrical variations to n_{eff} the dependency of n_{eff} on the microstructure scale has been computed by using the PCF cross-section of the two fibers via Comsol software (Fig. 5). A simulation based on the original image (corresponding to 100% in Fig. 5) yields a certain amount of n_{eff} (1.434 for #2 and 1.432 for #1). By varying the scale of the original SEM-image different values of n_{eff} are obtained and depicted in Fig. 5 for the two fibers.

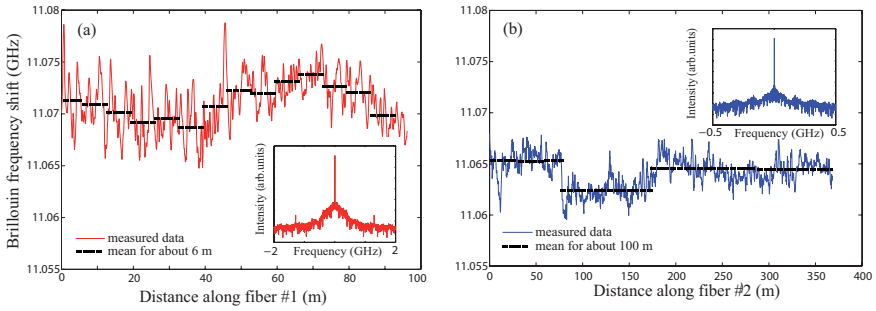

Fig. 4. Mapping of the Brillouin frequency shift along (a) fiber #1 and (b) fiber #2 showing the effect of inhomogeneities and strain. The insets show the Fourier transforms.

#130909 - $15.00 USD Received 29 Jun 2010; revised 31 Aug 2010; accepted 31 Aug 2010; published 7 Sep 2010

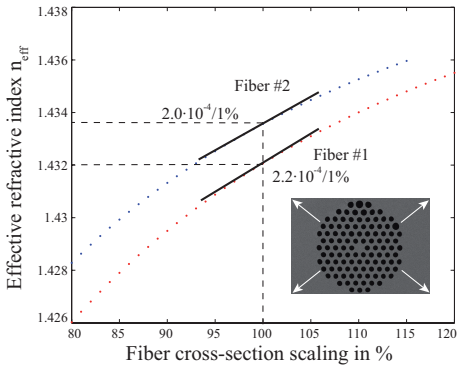

Fig. 5. Variation of the effective refractive index while tuning the scale of the SEM-image

We have computed the local derivation of the obtained relation between n_{eff} and the geometrical scale around 100% as indicted by the tilt solid lines in Fig. 5. The effective refractive index changes by $2.2 \cdot 10^{-4}$ (#1) and $2.0 \cdot 10^{-4}$ (#2) for 1%. This is compared to the fluctuations of the effective refractive index in the fibers under test by using Eq. (1). The variation of the short scale fluctuations (5±1 MHz for fiber #1 and 3±1 MHz for fiber #2) corresponds to 2.9±0.6% and 1.9±0.6% of scale or diameter fluctuations, respectively. The large scale variation is 4.7% (8 MHz for #1) and 3.2% (5 MHz for #2). This means that the maximum core diameter fluctuation is 5.5±0.3 μm (fiber #1) and 5.5±0.2 μm (fiber #2). Since polarization and strain can influence the variation of the effective refractive index the contribution of the structure size is expected to be below these values. This estimation confirms the higher quality of the drawing process obtained for fiber #2. Note that the fluctuations measured in the present work are in good agreement with the specifications from state-of-the-art PCF manufacturers [17, 18].

3. Conclusion

In this work we have proposed and demonstrated an useful technique mapping geometrical structure fluctuations along a photonic crystal fiber using Brillouin echoes distributed sensing. With this technique, we have been able to identify and quantify both long- and short-scale longitudinal fluctuations in the Brillouin frequency shift resulting from residual strain due to fiber coiling and air-hole microstructure or diameter fluctuations, respectively. The homogeneity of two photonic crystal fibers drawn from the same preform but with a different drawing process has been investigated and the fluctuations were logically found less important in the case of a fiber fabricated with a better process control. Our results finally demonstrate the great potential of the Brillouin echoes distributed sensing technique for small scale optical fiber characterization. Moreover, these results show the need for characterization of structural irregularities in fibers before they can be used for distributed sensing.

Acknowledgements

We thank the COST299 Action for financial support and V. Laude for helpful discussions. This work was funded by the European Interreg IV A program and the Fond Européen de Développement Régional (FEDER).

#130909 - $15.00 USD Received 29 Jun 2010; revised 31 Aug 2010; accepted 31 Aug 2010; published 7 Sep 2010